Pathways, timing, and evolution of Pacific Winter Water through Barrow Canyon

E. L. Shroyer[a,*], Robert S. Pickart[b]

[a] *Oregon State University*
[b] *Woods Hole Oceanographic Institution*

Abstract

Observations from a ship-based campaign in July-August 2009, combined with idealized numerical simulations, are used to investigate the seasonal delivery of Pacific Winter Water to Barrow Canyon and the subsequent adjustment of the flow down the canyon. As the current advects dense water, it transitions from a nearly barotropic structure near the canyon head to a strongly baroclinic flow with a subsurface maximum near the canyon mouth. Both the data and model indicate that the transit times along the three Chukchi shelf pathways feeding Barrow Canyon – a coastal pathway, a southern Hanna Shoal pathway, and a northern Hanna Shoal pathway – modulate the mode of winter water that occupies the canyon at a given time. In particular, remnant Pacific winter water carried along the rapid coastal pathway can precede the arrival of newly ventilated Pacific Winter Water carried along the two interior pathways. The observations and model indicate that the transition between water types draining from the canyon can occur rapidly over time scales of days to weeks. We also demonstrate that mixing along the path of the current is unlikely to result in the observed down-canyon transition from newly ventilated Pacific Winter Water to remnant winter water, further supporting the dominant role of advection. While the focus here is on the transition of winter water modes, the implication that seasonality within Barrow Canyon is tied to seasonality of the Bering Strait inflow, together with the relative transit times along advective pathways, should hold for other water types as well.

[*] *Corresponding author:* Emily Shroyer, Oregon State University, 104 CEOAS Administration Building, Corvallis, OR 97331-5503. Email: eshroyer@coas.oregonstate.edu

Keywords: Chukchi Sea, Barrow Canyon, Beaufort Sea, Pacific Winter Water, Alaskan Coastal Current

1. Introduction

Barrow Canyon, located in the northeast corner of the Chukchi Sea, is a primary route by which Pacific water exits the Chukchi Sea. As such it represents a critical control point for dictating the fate of this water in the western Arctic Ocean. North of Bering Strait, the flow of Pacific water across the Chukchi shelf is strongly influenced by topography and tends to follow three main pathways (Fig. 1). Barrow Canyon is located at the terminus of the easternmost pathway, which flows adjacent to the Alaskan coast. Some of the water transiting via the other two pathways, to the west through Herald Canyon and within the Central Channel (between Herald and Hanna Shoals, Weingartner et al. (2005)), is routed through Barrow Canyon as well. Observations (e.g., Weingartner, 2012) and model studies (Winsor and Chapman, 2004; Spall, 2007) suggest that Pacific water circulates clockwise around the northern bank of Hanna Shoal, with a portion diverted south of the shoal as well (Pickart et al., 2016, Fig. 1). These alternate routes then meet the coastal pathway near the head of Barrow Canyon and transit down the canyon. To the west of the canyon there is an eastward-flowing shelfbreak jet carrying Pacific water from the western-most pathway in Fig. 1 (Corlett and Pickart, 2017). Thus, Barrow Canyon represents a confluence of numerous branches of Pacific water on the northeastern Chukchi shelf.

At the mouth of the canyon Pacific water exits the Chukchi via different mechanisms. A portion of the water veers to the east and forms the Beaufort shelfbreak jet (Pickart et al., 2005a; Okkonen et al., 2009), although the transport of the jet only accounts for a small fraction of the Bering Strait inflow (Nikolopoulos et al., 2009; Brugler et al., 2014). Recently it has been documented that a substantial amount of the Pacific water turns to the west as it exits the canyon and forms a current over the Chukchi continental slope (Corlett and Pickart, 2017). Using a collection of shipboard transects occupied over more than a decade, Corlett and Pickart (2017) determined that the current is present in all wind conditions and transports ($\sim$0.5 Sv) of Pacific water westward. Mooring data have documented that the current, known as the Chukchi slope current, is present year-round (Li and Pickart, 2017). Pacific water can also exit Barrow Canyon via turbulent processes. The structure of the flow in the canyon satisfies the necessary conditions for baroclinic instability (Pickart et al., 2005a), and anti-cyclonic eddies (Pickart and Stossmeister, 2008) and filaments of Pacific water (Okkonen et al., 2009; Brugler et al., 2014) have been observed emanating from the canyon.

Water mass properties within the Chukchi Sea are set by advection through the Bering Strait in combination with local modification via air-ice-sea interaction, including ice formation and melt, and diapycnal mixing. In summer and early fall, the western side of Bering Strait typically contains nutrient- and carbon-rich Anadyr water, which has origins that extend to the Gulf of Anadyr in the northwest Bering Sea (Coachman et al., 1975). North of the strait this water mixes with Bering shelf water, derived from the central Bering Sea and northern Bering shelf, to form a water mass known as Bering summer water. (This water mass has also been called summer Bering Sea water, western Chukchi summer water, and Chukchi summer water.) During this time of year the eastern channel of the strait contains warm and fresh Alaskan Coastal Water, which is advected by the Alaskan Coastal Current (ACC). Progressing northward, the Bering summer water is found predominantly in the western and central pathways, while the Alaskan Coastal Water is confined mainly to the ACC. However, wind forcing can cause these two summer water masses to penetrate into different regions of the Chukchi shelf (Weingartner et al., 2005; Pisareva et al., 2015).

In winter and early-spring, a well-defined (in temperature and salinity space) water mass with temperatures near the freezing point flows through Bering Strait (Aagaard and Roach, 1990; Weingartner et al., 1998; Woodgate and Aagaard, 2005). We refer to this water mass as newly ventilated Pacific Winter Water (PWW), which is taken to be $< -1.65°$C. PWW is formed in the northern Bering Sea (Muench et al., 1988) and Chukchi Sea (Woodgate et al., 2005) during sea ice formation. It can also be further transformed on the Chukchi shelf within large polynyas (Weingartner et al., 1998; Itoh, M. and Shimada, K. and Kamoshida,

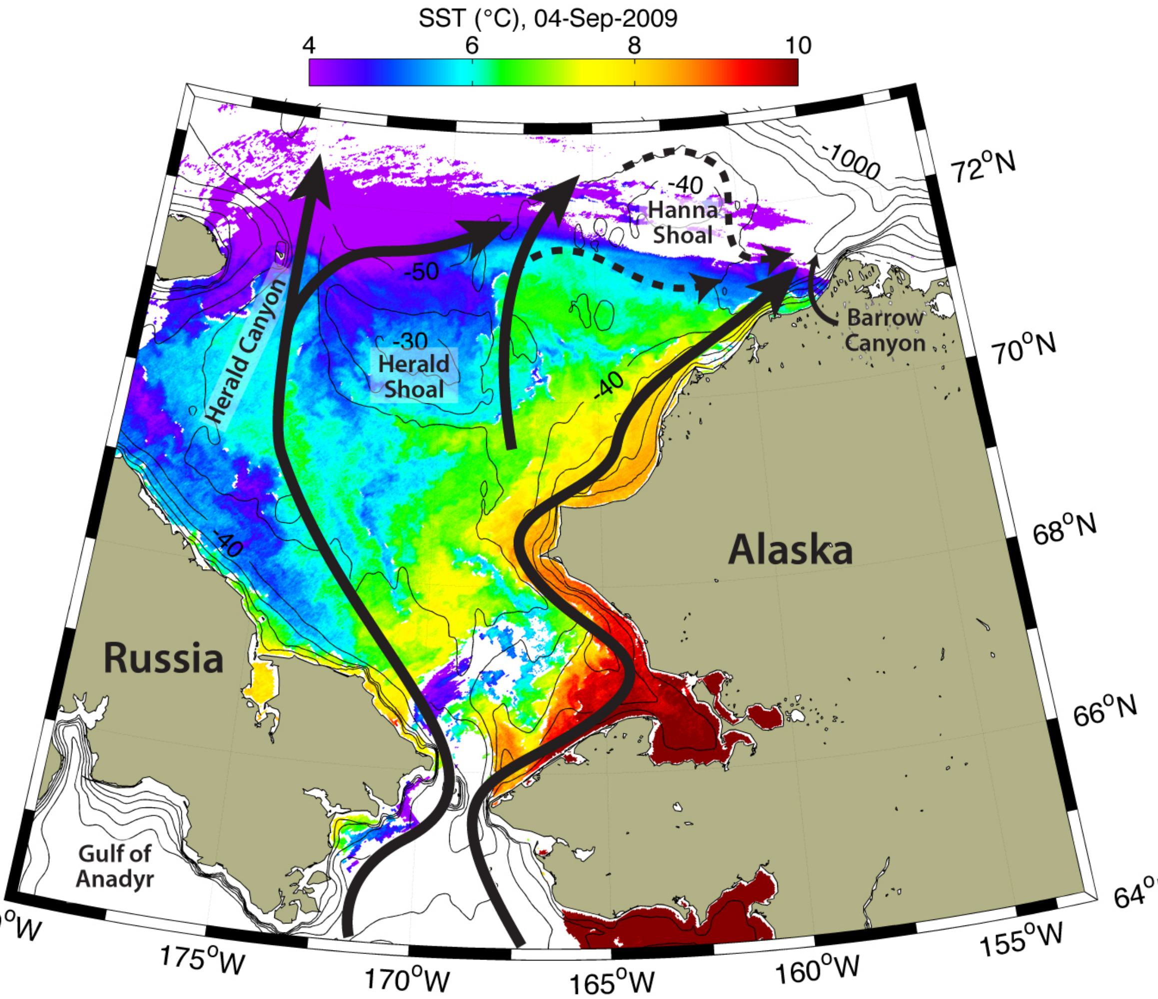

Figure 1: MODIS SST image for the Chukchi Sea taken on 4 September 2009, approximately one month after the shipboard survey was completed. This image highlights circulation paths within the Chukchi Sea, which are schematically indicated by arrows (and consistent with previous circulation diagrams, e.g. Gong and Pickart, 2015). The dashed arrows near the northeast corner indicate circulation around Hanna Shoal.

T. and McLaughlin, F. and Carmack, E. and Nishino, S., 2012) and within smaller leads and openings (Pacini et al., this issue). If the transformation is extensive enough, the water is classified as "hypersaline" winter water ($\gtrsim 34$). This salty and dense variety of winter water is at times observed flowing northward through Barrow Canyon (Itoh, M. and Shimada, K. and Kamoshida, T. and McLaughlin, F. and Carmack, E. and Nishino, S., 2012), and it can also be upwelled from the Beaufort into the canyon (Pisareva et al., this issue). After winter, PWW is warmed by mixing and/or solar heating (e.g., Gong and Pickart, 2015). We refer to this modified product as Remnant Winter Water (RWW), which is taken to be in the temperature range -1 to -1.65°C. This water comprises the bulk of the upper portion of the cold halocline throughout the western Arctic Ocean (Steele et al., 2004). However, hypersaline winter water that is dense enough can ventilate the lower halocline as well (Spall et al., 2008).

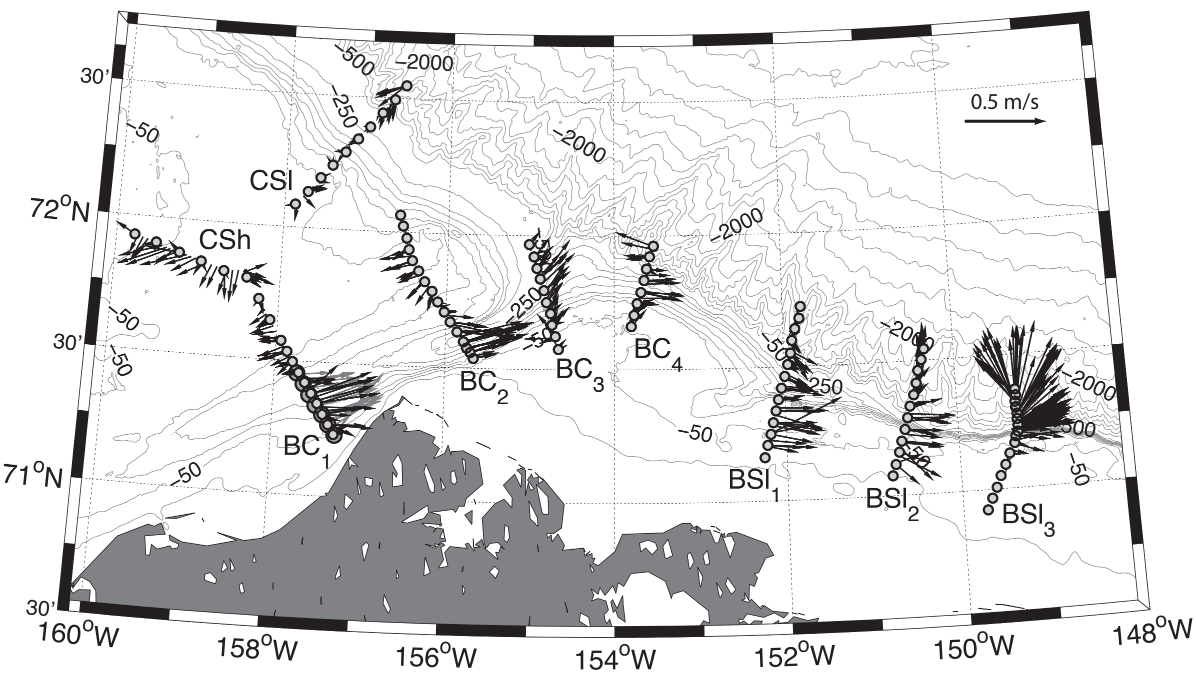

Figure 2: Map of the observational study area showing the locations of the CTD profiles occupied during the cruise (grey circles). Hydrographic/velocity transects were made over the Chukchi Shelf (CSh), across the Chukchi Slope (CSl), within Barrow Canyon (BC), and across the Beaufort Slope (BSl). The vectors denote the depth mean (to a maximum of roughly 250 m) velocity from the vessel-mounted acoustic Doppler current profiler. The BC_1 transect was occupied twice (dark and light grey circles, grey and black vectors), near the beginning and end of the cruise.

Spatial and temporal variability in both inflow and water mass composition at Bering Strait, combined with a large range in residence times within the Chukchi Sea (from a few months to a year according to Spall (2007)), create the potential for storage, modification, and mixing of various Pacific water masses within the Chukchi Sea. This is particularly true in Barrow Canyon where the multiple pathways reunite. As such, it is common for winter and summer water masses to co-exist within the canyon (e.g., Pickart et al., 2005b; Shroyer, 2012; Pickart et al., this issue). For example, Pickart et al. (2005b) examined two sections occupied across the canyon during a time when both the ACC was present as well as a deeper flow of PWW. They observed that the layer of PWW adjusted via deceleration and stretching as it descended down-canyon; their analysis also indicated that hydraulic control and/or mixing may be important processes within Barrow Canyon. This survey was limited to two across-canyon transects– one upstream of the head of the canyon (~ 50 km upstream of transect BC_1 in Fig. 2) and the second near the Chukchi-Baufort shelfbreak (near transect BC_2 in Fig. 2).

Both the seasonality and synoptic variability of the circulation in Barrow Canyon is largely attributable to the winds (Weingartner et al., 1998; Okkonen et al., 2009). The prevailing winds are northeasterly and tend to retard the mean flow. During summer, when these prevailing winds are weakest, the northward transport through the canyon is maximum (Itoh, M. and Shimada, K. and Kamoshida, T. and McLaughlin, F. and Carmack, E. and Nishino, S., 2012; Weingartner et al., 2017). Based on a 36-year wind-transport hindcast at the head of the canyon, Weingartner et al. (2017) argues that there is weak southward transport during the fall and near-zero transport during winter. On shorter timescales, upwelling favorable winds arise due to the influence of both the Beaufort High and Aleutian Low (Weingartner et al., 2017; Pisareva et al., this issue; Pickart et al., this issue). Using two years of mooring data near the head of the canyon, Pisareva et al. (this issue) found that the most common water mass upwelled from the basin was cold winter water (both PWW and RWW). At times, however, the winds drive Atlantic water from the lower halocline into the canyon (e.g., Mountain et al., 1976; Münchow and Carmack, 1997; Weingartner et al., 1998). The upwelling of Atlantic water occurs most often during the late fall to early spring (Pisareva et al., this issue), likely because the Pacific-Atlantic water interface seaward of the canyon is shallower at this time of year, making the Atlantic water more accessible (Lin

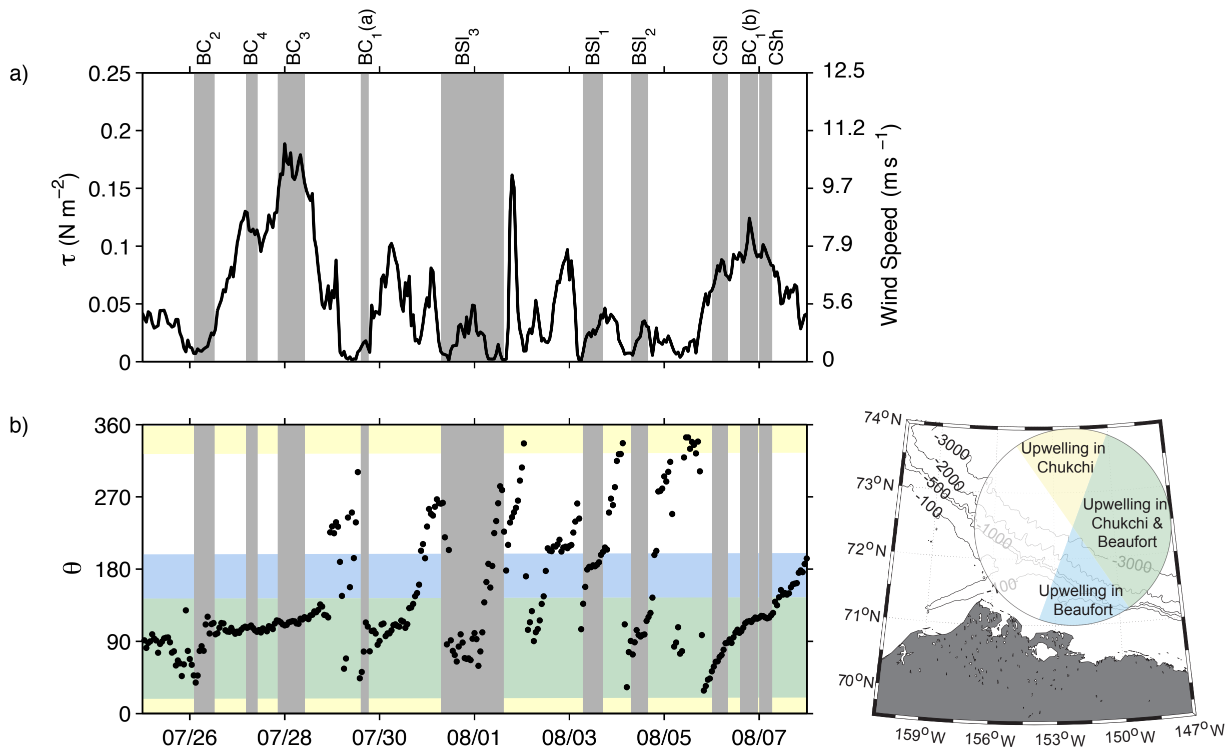

Figure 3: a) Wind stress and b) direction (from which the winds are blowing) during the cruise using the Barrow weather station data. The time periods of the CTD transect lines are shaded in grey and labeled at the top. Colored bands in the bottom panel denote approximate regions of upwelling favorable winds for the Beaufort Alaskan coast (blue), Chukchi Alaskan coast (yellow), and both coasts (green), as defined within the map inset.

et al., this issue). Occasionally, Atlantic Water intrudes far onto the Chukchi shelf (Bourke and Paquette, 1976; Ladd et al., 2016).

The motivation for the present study is to enhance our knowledge of the timing of winter water delivery to Barrow Canyon and the subsequent adjustment of the flow down the canyon. Since the winter water is high in nutrients, it is especially important for the ecosystem of the Chukchi shelf as it supports the growth of phytoplankton at the base of the food web (Codispoti et al., 2005; Hill and Cota, 2005; Lowry et al., 2015). There are specific areas on the northeast Chukchi shelf and in Barrow Canyon that are characterized as "hot spots", i.e. regions of increased biological activity and enhanced benthic biomass (e.g., Hill and Cota, 2005; Grebmeier et al., 2015). In part to learn more about these and other hot spots in the northern Bering Sea, Chukchi Sea, and Beaufort Sea, the Distributed Biological Observatory (DBO) program was established in 2010 (Moore and Grebmeier, 2017). The premise of DBO is to collect timeseries in such critical locations to further our understanding of the physical-biological links involved and how the hot spots might change as the climate continues to warm. Two of the DBO lines, DBO4 and DBO5, are located southeast of Hanna Shoal and in Barrow Canyon, respectively. Consequently, it is of considerable interest to understand the various factors that dictate the supply of winter water to these regions, which is addressed in the present paper.

We focus on the evolution and dynamics of the winter water (PWW and RWW) as it approaches and exits Barrow canyon under weak atmospheric forcing in summer. We use data from a 2009 hydrographic/velocity survey that captured dense PWW descending down Barrow Canyon, transitioning from a nearly barotropic structure to one with pronounced baroclinicity characterized by a sub-surface current maximum. To complement the data analysis, we use a simplified numerical model to investigate the transit times in the Chukchi Sea and the arrival of various water masses within Barrow Canyon. The measurements are detailed in Section 2. An overview of the wind field and component water masses is presented in Section 3. The observational analysis appears in Section 4, and a comparison with the results of the model is presented in Section 5.

2. Measurements

From 26 July – 7 August 2009, ten hydrographic/velocity sections were occupied in the vicinity of the shelf edge in the eastern Chukchi and western Beaufort Seas from the USCGC *Healy*. Locations of the Conductivity-Temperature-Depth (CTD) profiles are shown in Figure 2. The station spacing ($\lesssim 5$ km) was sufficient to resolve the internal deformation radius which is less than 10 km in this region. The transects are labeled according to their geographic location as follows: Chukchi Shelf (CSh), Chukchi Slope (CSl), Barrow Canyon (BC), and Beaufort Slope (BSl). Numerical subscripts of the sections increase moving

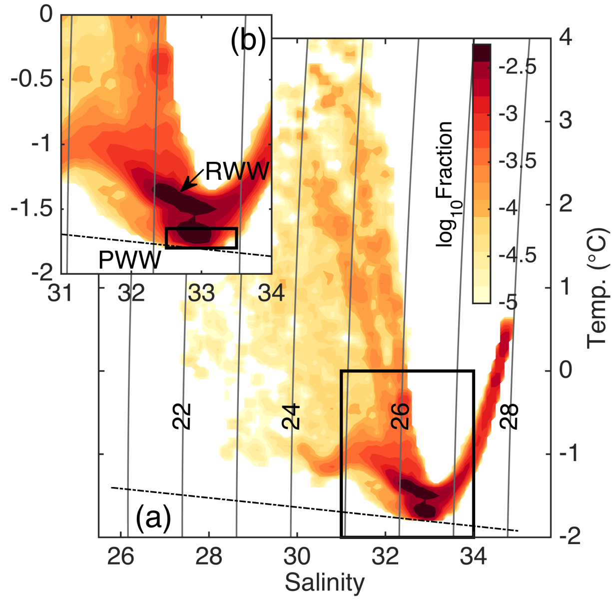

Figure 4: a) TS-histogram plot for depths shallower than 250 m from all sections. b) Enlarged view highlighting the bimodal structure of the Pacific Winter Water. PWW = newly ventilated winter water; RWW = Remnant Winter Water. The freezing point at the surface is shown in black (dash-dot).

downstream (i.e., in the direction of propagation of coastally trapped waves). Transect BC_1 was sampled twice, once near the beginning of the survey (large dark grey circles) and once near the end of the cruise (small light grey circles). Two transects were occupied to the west of Barrow Canyon. Transect CSh was the extension of the $BC_1(b)$ transect, positioned between the offshore flank of Barrow Canyon and Hanna Shoal, and transect CSl was occupied across the Chukchi slope. Three transects were made to the east of Barrow Canyon across the Beaufort slope ($BSl_{1,2,3}$).

The *Healy* was equipped with a Sea-Bird Electronics SBE 9*plus* CTD with dual temperature and conductivity sensors. Based on laboratory calibration, the temperature accuracy is estimated to be 0.001°C, and, based on calibration with in-situ water samples, the salinity is deemed accurate to 0.008 on the shelf and 0.002 in deep water. The CTD downcast data were averaged into 1-m bins that were then used to calculate potential temperature (hereafter referred to simply as temperature), potential density (referred to as density), and buoyancy frequency (N^2).

Velocity data were collected using a vessel-mounted RD Instruments (RDI) 75 KHz Acoustic Doppler Current Profiler (ADCP), configured to obtain 5-minute averaged profiles with a vertical bin size of 8 m. The data were acquired using the VMDAS software, and were processed post-cruise using the the University of Hawaii software package CODAS. Data were flagged for outliers using standard RDI metrics (percent good and backscatter). The barotropic tidal signal was removed from the velocity profiles using the Oregon State University barotropic tidal prediction model (Padman and Erofeeva, 2004). The profiles along each transect were then rotated into along- and across-stream components by minimizing the magnitude of the vertically averaged cross-stream velocity. The upper-most velocity bin is at 24 meters depth. In order to calculate along-stream transports, we integrate the geostrophic velocity computed using the measured thermal wind shear referenced to the measured depth-averaged along-stream velocity (i.e., the average between upper-most and the lower-most ADCP bin). The estimated transports are therefore equivalent to the measured transports over the resolved depth-range of the ADCP, while the vertical distribution of geostrophic transports may vary from those estimated from the measured velocity. The standard deviation between the measured along-stream velocity (smoothed over 4 km) and the geostrophic estimate is less than 5 cm s^{-1} for all transects within Barrow Canyon with the exception of BC$_3$. Uncertainty in BC$_3$ approaches 15 cm s^{-1} (standard deviation); however, the difference is greatest offshore of $\sim$ 37 km (i.e., where the transect is no longer oriented across-isobath). Neglecting this region the standard deviation between the measured along-stream velocity and the geostrophic estimate is 7 cm s^{-1} for this transect.

Turbulent kinetic energy (TKE) dissipation, ϵ (W kg^{-1}), was estimated from Thorpe overturns calculated from 10-cm averages of density, i.e., a smaller vertical binning interval is used for the purpose of quantifying mixing (Thorpe, 1977). Processing of Thorpe overturns (L_T) followed Galbraith and Kelley (1996), and L_T smaller than that resolvable given sampling constraints were discarded. Two limiting values were used. The first, 0.5 m ($5\delta z$), is related to the vertical sampling; and the second, $(2\frac{\delta\rho}{\delta\rho_0/\delta z})$, where $\delta\rho_0/\delta z$ is the mean (sorted) density gradient through the overturn, depends on the density resolution of the sensor ($\delta\rho \sim 0.001$ kg m^3). In addition, a run length criterion was imposed in which the length of points within an overturn was required to exceed that likely to occur for random noise (Galbraith and Kelley, 1996). Dissipation was calculated using $\epsilon = L_O^2 N^3$ where $L_O \sim 0.8 L_T$ is the Ozmidov scale (Dillon, 1982).

3. Observational Context

At the time of the survey, a well-defined coastal current transported water out of the Chukchi Sea through Barrow Canyon and continued along the Beaufort slope (Fig. 2). Ideally, these sections would constitute a synoptic realization. In order to assess this potential, we first consider the wind forcing during the cruise, as well as upstream influences (e.g., advection of different water masses or shelf wave propagation). The former can be evaluated using the meteorological data measured at the Barrow, Alaska Observatory (`/www.esrl.noaa.gov/gmd/obop/brw`). With regard to the latter, examination of temperature/salinity (TS) properties provides some guidance as to the importance of upstream advection, at least in terms of transport of heat and salt. Before analyzing the circulation and water mass evolution using the shipboard data, we first document the local wind forcing and overall TS properties measured during the survey.

3.1. Winds

Although variable during the survey period, winds were of moderate amplitude (Fig. 3a) and predominantly directed from the northeast-east (Fig. 3b). This direction corresponds to generally upwelling-favorable conditions for Barrow Canyon and the Beaufort slope. Individual wind events typically lasted a few days. Previous analysis of data from the Barrow Observatory suggest that such moderate wind events are typical this time of year (Shroyer and Plueddemann, 2012), while strong summertime upwelling events are uncommon (Pisareva et al., this issue). Based on oceanographic mooring data, flow reversals in Barrow Canyon tend to occur once the upcanyon component of the wind exceeds $5-6$ m s^{-1} (Weingartner et al., 1998; Pisareva et al., this issue). While Fig. 3 suggests that several of the

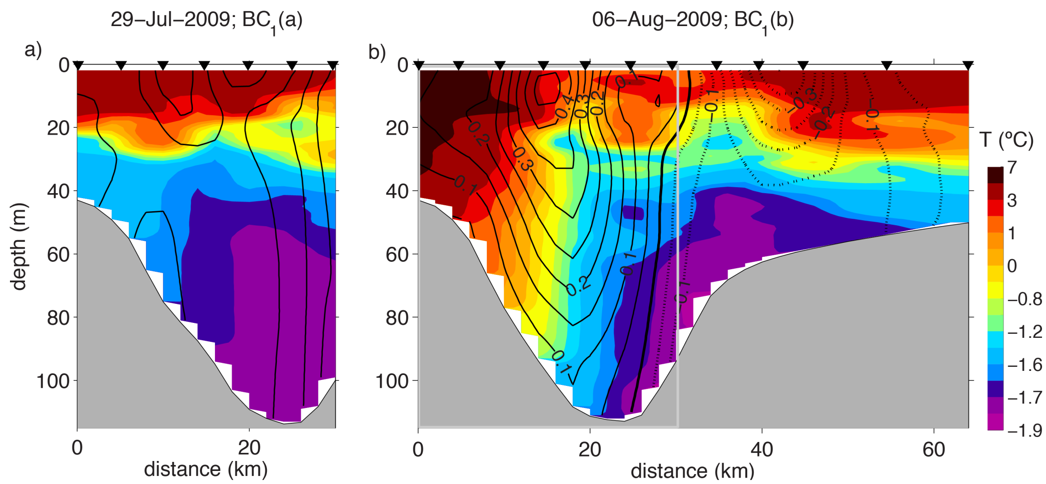

Figure 5: Temperature (color) and velocity (m s^{-1}, contours) for the two upper canyon transects, a) BC_1(a) and b) BC_1(b). Note that the temperature color scale is nonlinear and designed to highlight PWW (dark blue-purple). The grey line in BC_1(b) denotes the geographical extent of BC_1(a). Distance increases moving offshore from the Alaskan coastline. Positive velocity (solid contours) is directed downstream out of the Chukchi Sea; negative velocity (dashed contours) is directed upstream into the Chukchi. The zero velocity contour is shown in bold.

canyon sections were subject to upwelling favorable winds, the along-canyon wind component did not exceed 5 m s^{-1} during the any of the canyon transects. For the Beaufort slope, the shelfbreak jet tends to reverse for along-coast winds exceeding 4 m s^{-1} (although this is not always the case, Schulze and Pickart (2012)). The only transect where this condition was met was BC_4 (just beyond the mouth of Barrow Canyon). However, the winds ramped up very quickly prior to the occupation of the section, and the current likely did not have time to respond. As shown below, flow reversals along the winter water pathway were not observed in any of the sections, and the associated current transports were consistent with one another throughout the survey. As such, we assume that the survey captured a primarily unforced state of the boundary current system.

3.2. Water Mass Properties

The TS distribution for depths less than 250 m is shown in Figure 4. Cold and relatively fresh TS values (lower left portion of 4a) are likely a mixed-meltwater product. Warm, fresh

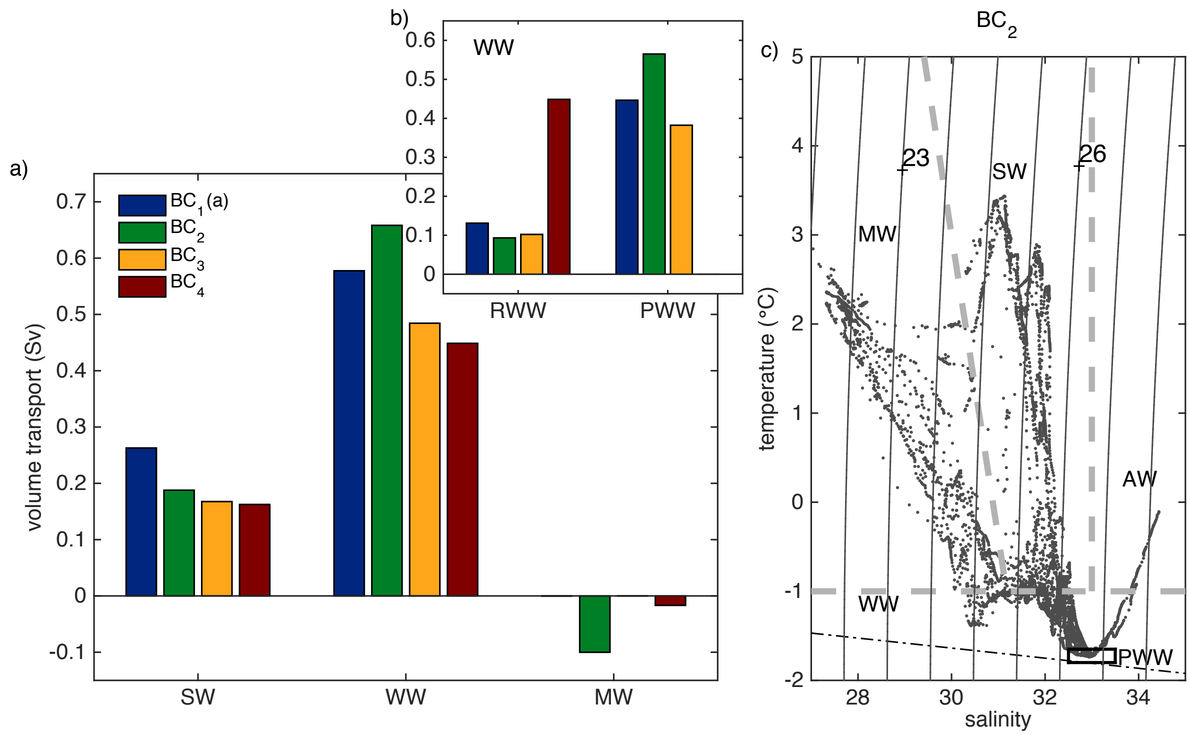

Figure 6: a) Volume transport by TS class for the four CTD sections in Barrow Canyon: BC_1(a), BC_2, BC_3, and BC_4. b) Inset showing the division of Pacific Winter Water (WW) into newly ventilated winter water (PWW) and Remnant Winter Water (RWW). c) TS plot for the BC_2 transect showing the water mass classes defined in the text: summer water (SW), modified meltwater (MW), Atlantic water (AW), and WW (the PWW subclass is denoted by the box). The freezing point at the surface is shown in black (dash-dot).

values (upper left corner of Fig. 4a) are consistent with the properties of Alaskan Coastal Water. Volumetrically, the contribution from Alaskan Coastal Water was small; only the second occupation of BC_1 showed the presence of this water mass. Accordingly, this transect is not considered synoptic with the remaining sections. Inclusion of all depths in the TS histogram (not shown) indicates that roughly 50% of the observations are confined within a TS-mode near 0.5 °C and 35, characteristic of Atlantic water that is prevalent in the deep portion of the sections across the Chukchi and Beaufort slopes.

The bulk of the TS measurements above 250 m were associated with the cold and moderately salty winter water that was present during the hydrographic survey (highlighted in

Fig. 4b). Two distinct cold TS-modes were sampled: a lower peak representing PWW and an upper peak encompassing RWW. Transects $BC_{(1-3)}$, CSh, and CSl, with geographical ties to the Chukchi Sea, contributed the most to the PWW peak. In contrast, the coldest waters observed in sections $BSl_{(1-3)}$ and BC_4 were slightly warmer and located in the upper RWW mode. This geographical distribution of the two types of winter water is suggestive of at least two possibilities. The first interpretation is that PWW is transformed via mixing into RWW along the path of the current as it emanates from the canyon, and that our survey encompassed the segment of the current over which this modification takes place. The second possibility is that, at the time of the survey, PWW was just beginning to flow through the canyon. The latter interpretation is consistent with the results of Pickart et al. (this issue) who deduced that PWW is delivered to the canyon at this time of year via the slower pathways on the interior shelf (around Hanna Shoal). In that scenario, our survey captured the "front" between the RWW, which previously had been streaming out of the canyon from the coastal pathway, and the PWW that arrived later via the longer pathway. Below we shed light on this issue by investigating the mixing implied by the measurements, and the timing of the PWW pathways using the numerical model.

4. Measurements in Barrow Canyon

Based on the observed wind forcing and TS measurements, we consider the CTD transects $BC_1(a)$, BC_2, BC_3, and BC_4 to be quasi-synoptic. Before presenting the analysis of these sections, we first compare transects $BC_1(a)$ and (b), which demonstrate how advection from upstream sources can profoundly influence the region on short timescales.

4.1. Comparison of Upper Canyon Transects

Figure 5 compares the vertical sections of temperature and alongstream velocity for the two BC_1 transects, which were separated by roughly one week. In both cases, the near-surface water is relatively warm (> 3°C) and the maximum current speed is in excess of 0.5 m s^{-1}. However, pronounced differences are apparent in the two sections. The 29 July 2009 transect consisted largely of PWW. (In this figure and others to follow, the PWW

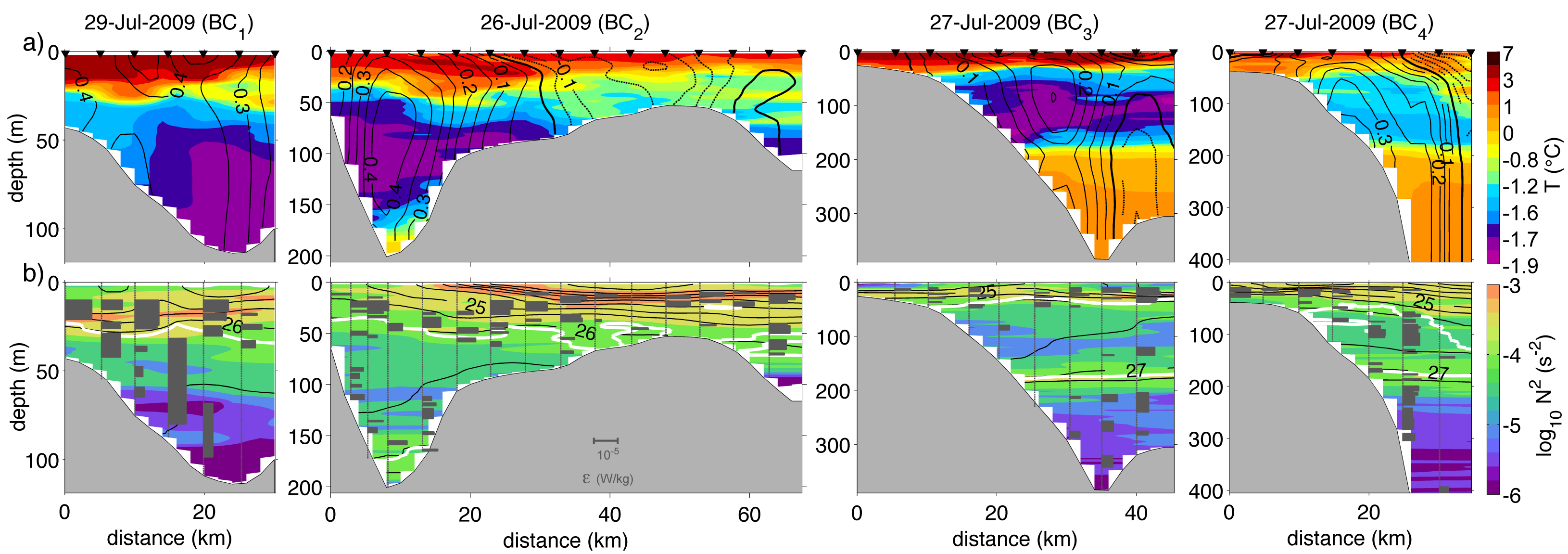

Figure 7: a) Temperature (color) overlain by geostrophic velocity (contours, m s^{-1}) and b) $\log_{10}N^2$ (color) for the BC_1(a), BC_2, BC_3, BC_4 transects. In panel b, the thick white contours denote the $-1.2°C$ isotherms which approximately bracket the Pacific Winter Water layer; the black contours are density kg m^{-3}. The turbulent kinetic energy dissipation rate (from a Thorpe scale analysis) is indicated by the grey bars.

corresponds to the dark blue and purple colors, i.e. colder than -1.65°C.) By contrast, the 6 August 2009 transect recorded the presence of very warm Alaskan Coastal Water at the western four stations, extending as deep as 80 m. The structure of the down-canyon flow was also markedly different between the two occupations. The 29 July current was more barotropic, and the 6 August current was strongly baroclinic. It is clear that the ACC was present on the eastern flank of the canyon during the second realization.

During the re-occupation of this section, measurements were taken beyond the canyon rim onto the Chukchi shelf (Fig. 2). Offshore, the section shows a surface-intensified, southward-flowing current associated with a hydrographic front just beyond the western wall of the canyon. The swift part of the current is advecting warm water, while the base of the jet contains PWW. We suspect that this is the Pacific Water pathway that extends northward through Central Channel and bends anti-cyclonically around Hanna Shoal (see Fig. 1). Note that the southward-flowing PWW is not constrained to the shelf region between Hanna Shoal and Barrow Canyon, i.e. a portion extends down into the canyon (Fig. 5 b). This signature may be the eastward-flowing Chukchi shelfbreak jet being diverted along the isobaths into Barrow Canyon. This interpretation is also consistent with the southward flow along the western half of BC_2 (Fig. 2). In any event, these flows provide a source of PWW into Barrow Canyon late in the season, well after the Alaskan coastal pathway would have advected such cold water through the canyon (see also Pickart et al., this issue).

The change from the down-canyon flow of PWW in the first realization to the appearance of the ACC in the second realization is clearly associated with advection from the Chukchi shelf. Mooring data from within Barrow Canyon suggest that this transition can be quite abrupt. For example, (Mountain et al., 1976) note an increase of 4.5°C in less than 48 hours. The comparison above highlights one of the difficulties in treating shipboard sections acquired in this region as synoptic, especially when the timing of those sections is not consistent with the progression of the flow. Temporally, we sampled in the following order: BC_2, BC_4, BC_3, and $BC_1(a)$ due to logistical constraints imposed by mooring operations on the cruise. While this is not ideal, analysis of the transports and properties (Section 4.2) supports the

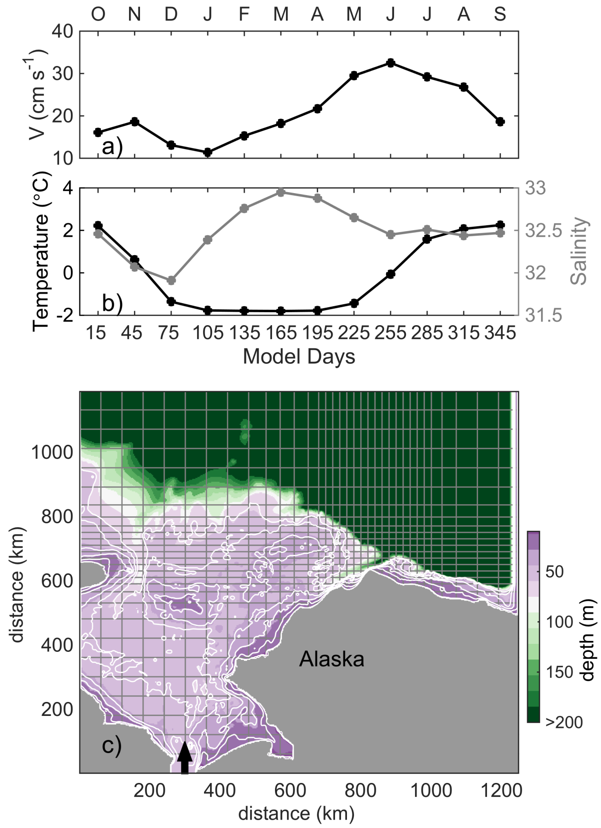

Figure 8: Model forcing and domain. The seasonal cycle model is forced at Bering Strait with a spatially-homogeneous signal in a) velocity and b) temperature-salinity. The model domain (c) is non-uniform, with the highest lateral resolution centered in Barrow Canyon. Grid boundaries are plotted in grey at an interval of 20 cells. The bathymetry (m) is colored, with contours plotted every 10 m from 10 to 60 m depth in white.

assumption of near-synopticity for these four transects.

4.2. Evolution of the Flow through Barrow Canyon

We begin the analysis of how the flow evolves through the canyon by considering volume transports separated into TS classes for the four near-synoptic sections (Fig. 6a). For this analysis, positive transports are directed out of the Chukchi Sea, and water mass classes were defined based on the character of the TS plots. A representative TS diagram from BC_2 is shown in Fig. 6c. As discussed above, water with temperature less than -1°C was classified as winter water (PWW or RWW). Water warmer than this limit was sorted into three groups:

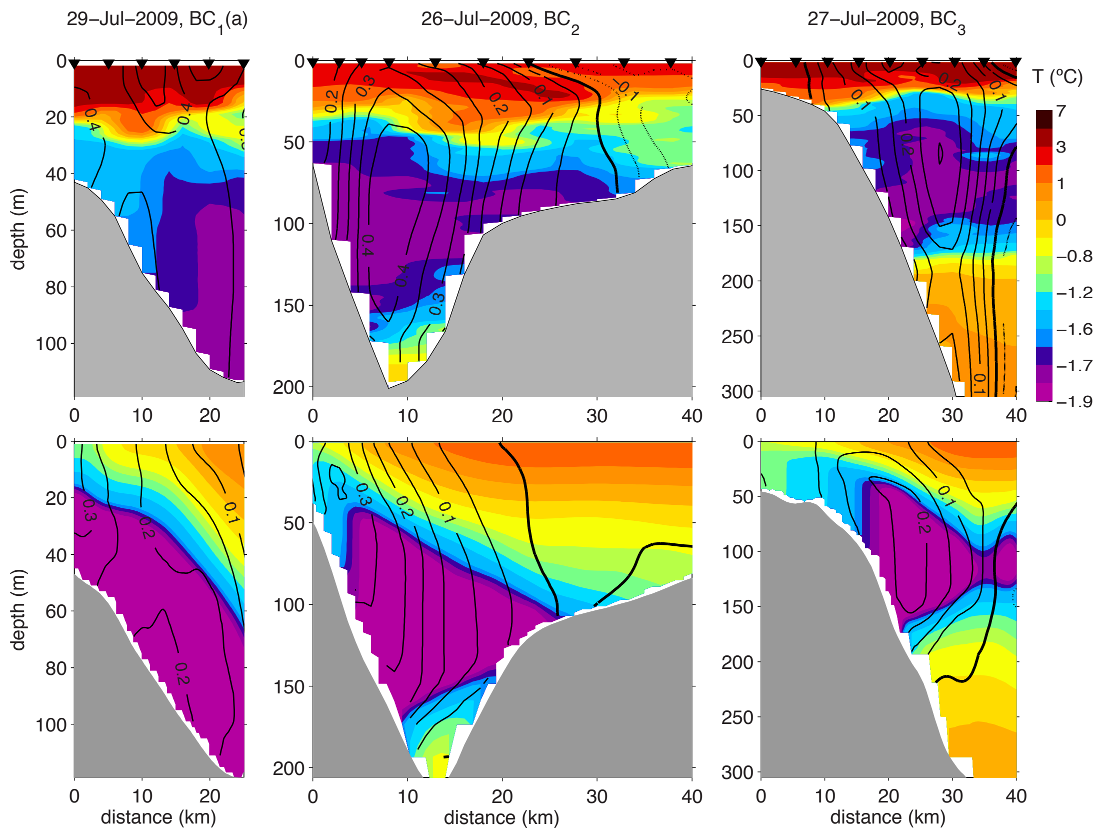

Figure 9: Comparison of the observations and the model (snapshot from the winter water simulation) along three transects through Barrow Canyon. The color is temperature (°C) and the contours are alongstream velocity (m s^{-1}) with the old contour showing the zero velocity contour 0 m s^{-1}. The model transects were sampled along similar latitude and longitude lines.

modified meltwater (MW), summer water (SW, predominantly Bering summer water), and Atlantic water (AW). The first two classes are separated from AW using a constant salinity of 33. A linear relation between temperature and salinity (diagonal line shown in Fig. 6c) was used to separate SW and MW, with the fresher, colder branch being attributed to MW. We note that various TS definitions have been applied in the literature to describe the regional water masses of the Chukchi and Beaufort Seas in detail. The boundaries adopted here are meant to characterize the broad water types; small variations to these definitions do not change our conclusions given the types of water sampled in this shipboard survey. The combination of the two winter water masses is referred to below as WW.

The total transport of WW and SW out of the Chukchi Sea (i.e., the sum of the positive bars for each transect) was nearly identical for $BC_1(a)$ and BC_2 at 0.85 Sv, and slightly less for BC_3 and BC_4 at ~ 0.65 Sv and 0.58 Sv, respectively. We note that BC_3 and BC_4 also transported roughly 0.08 Sv and 0.17 Sv of AW in the upper 250 m; these values are not represented in Fig. 6a. (The transport of AW in $BC_1(a)$ and BC_2 is negligible.) BC_2, which was the only transect of this set that extended onto the Chukchi shelf offshore of Barrow Canyon, shows transport of MW to the southwest. Although differences are apparent, the relative amounts of SW (~ 0.2 Sv) and WW (~ 0.5 Sv) are consistent among these four transects. The primary difference is that the winter water transport in the first three sections consisted primarily of PWW, while in the fourth section it was comprised entirely of RWW (Fig. 6b).

The evolution of the flow through the canyon is effectively visualized by comparing vertical sections of the four transects (Fig. 7 with the $-1.2°$C isotherms in white delimiting the WW). It is seen that SW is found near the surface in all of the sections. The first transect $BC_1(a)$, in the upper portion of Barrow Canyon, is dominated by outflow of PWW that is in contact with the bottom. The isopycnals are relatively flat and, as such, there is little vertical structure to the flow. A marked transition takes place between this transect and the next one (BC_2). One sees that the layer of PWW has descended and stretched so that it now extends down to 150 m, lying above the deep Atlantic layer. The other significant change is that the isopycnals that bound the PWW are now strongly sloped. In particular, they diverge as one progresses from the western side of the canyon to the eastern side. This results in a mid-depth intensified jet. Interestingly, at the offshore end of this transect there is weak flow of PWW approaching Barrow Canyon along the Chukchi slope. This supports the notion that some of the PWW seen progressing into the canyon in section $BC_1(b)$ has emanated from the Chukchi shelfbreak jet.

The third transect, BC_3, is at the canyon mouth (Fig. 2), and the conditions here are not very different from the preceding section. The PWW layer is similar in structure and the cold jet remains mid-depth intensified. More of the Atlantic layer is sampled in this section, and

	BC_1(a)	BC_2	BC_3	BC_4
Min	$8.4 \cdot 10^{-9}$	$4.4 \cdot 10^{-9}$	$2.0 \cdot 10^{-8}$	$1.2 \cdot 10^{-8}$
Max	$6.6 \cdot 10^{-5}$	$5.3 \cdot 10^{-5}$	$2.1 \cdot 10^{-5}$	$2.8 \cdot 10^{-5}$
Median	$9.8 \cdot 10^{-7}$	$1.4 \cdot 10^{-6}$	$6.5 \cdot 10^{-8}$	$6.5 \cdot 10^{-7}$
Mean	$8.7 \cdot 10^{-6}$	$5.7 \cdot 10^{-6}$	$1.4 \cdot 10^{-6}$	$3.0 \cdot 10^{-6}$

Table 1: Turbulent kinetic energy dissipation estimates for BC_1(a), BC_2, BC_3, BC_4 transects in W kg^{-1} from the Thorpe Scale analysis. The means and medians are calculated for detectable values over the water column; they will be high given that low values of ϵ are not included in the estimate.

there is a reversal in the deep isopycnal slope associated with an enhanced flow of this warm water in the same direction as the PWW. The final transect BC_4 is beyond the canyon and crosses the Beaufort slope. Again there is marked change, both in the hydrography and in the flow. Notably, there is no PWW present in the section, only RWW. Also, the isopycnals are now uniformly sloped so that the sense of thermal wind shear is the same throughout the water column; accordingly, the jet of cold water is now bottom trapped. Note that the strongest flow of winter water is found roughly 100 m deeper at BC_4 than at the previous two sections ($\sim$180 m versus $\sim$80 m). Overall then, our survey showed that the flow of winter water emanating from Barrow Canyon moderated in its properties – changing from PWW to RWW – and transitioned from a nearly barotropic structure at the canyon head to being mid-depth intensified, and, finally, becoming bottom-intensified along the Chukchi slope.

The turbulent kinetic energy dissipation from the four transects is estimated using a Thorpe scale analysis (Figure 7b) with the intent of bounding the degree of mixing between SW and PWW within Barrow Canyon. The use of Thorpe scales limits the calculation of dissipation to regions where resolved overturns are detected and, consequently, sets a minimum on the observable dissipation rate. Even though energy constraints suggest that overturns occur more easily in weak stratification, they are more difficult to detect given the resolution of the CTD. Accordingly, a tendency for enhanced dissipation to occur in regions of increased stratification is evident in Fig. 7b. Mean, median, and extreme values are presented in Table 1. Note that the means and medians would be considerably lower if we replaced non-resolvable values with a "noise floor", e.g., 10^{-10} W kg^{-1}. Regardless of any relative sensitivity, in this series of transects the mixing between summer and winter water tended to be greatest in the upper to mid canyon and decreased as the water transited through the mouth. This trend is consistent with direct microstructure estimates from Barrow Canyon that were collected along the periphery of Barrow Canyon in September 2010 (Shroyer, 2012).

Dissipation can be converted to a turbulent diffusivity using $K = \Gamma\epsilon/N^2$ with the mixing efficiency Γ assumed to be equal to 0.2. This relationship yields an upper bound on the mean K within ± 5 m of the upper -1°C isotherm (i.e., the SW/WW boundary) of roughly 5×10^{-4} m^{2}s^{-1} over the upper three transects. Diffusivity along BC_4 is considerably lower at 10^{-7} m^{2}s^{-1}. (For the mean estimates of diffusivity a molecular noise floor is assumed.) These estimates of diffusivity compare reasonably well to the median values of diffusivity given in Shroyer (2012), which ranged from 3×10^{-4} m^{2}s^{-1} in the upper canyon to 4×10^{-7} m^{2}s^{-1} in the lower canyon.

Assuming a constant diffusivity of 5×10^{-4} m^{2}s^{-1} applied to a two-layer interface between SW at nominally 4°C and PWW at nominally -1.8°C, a one-dimensional mixing model suggests that a roughly 15-m layer of RWW can be created over two days (roughly equivalent to the advective timescale for the transit between BC_1(a) and BC_3). Note that this estimate is merely illustrative of the potential for diapycnal mixing to be a significant contributor to water mass evolution within the canyon. It is oversimplified, notably by neglecting pre-existing gradients between SW and PWW (i.e., the initial condition is not two-layer), and in the inability of sparse Thorpe-scale estimates to adequately resolve intermittent turbulent events in order to yield robust mean mixing values. Nonetheless, despite these limitations, this simple estimate strongly suggests that the abrupt transition between PWW and RWW observed between BC_3 and BC_4 in the shipboard survey is not attributed to vertical mixing alone as RWW spans a $\sim$ 100-m thick layer in BC_4.

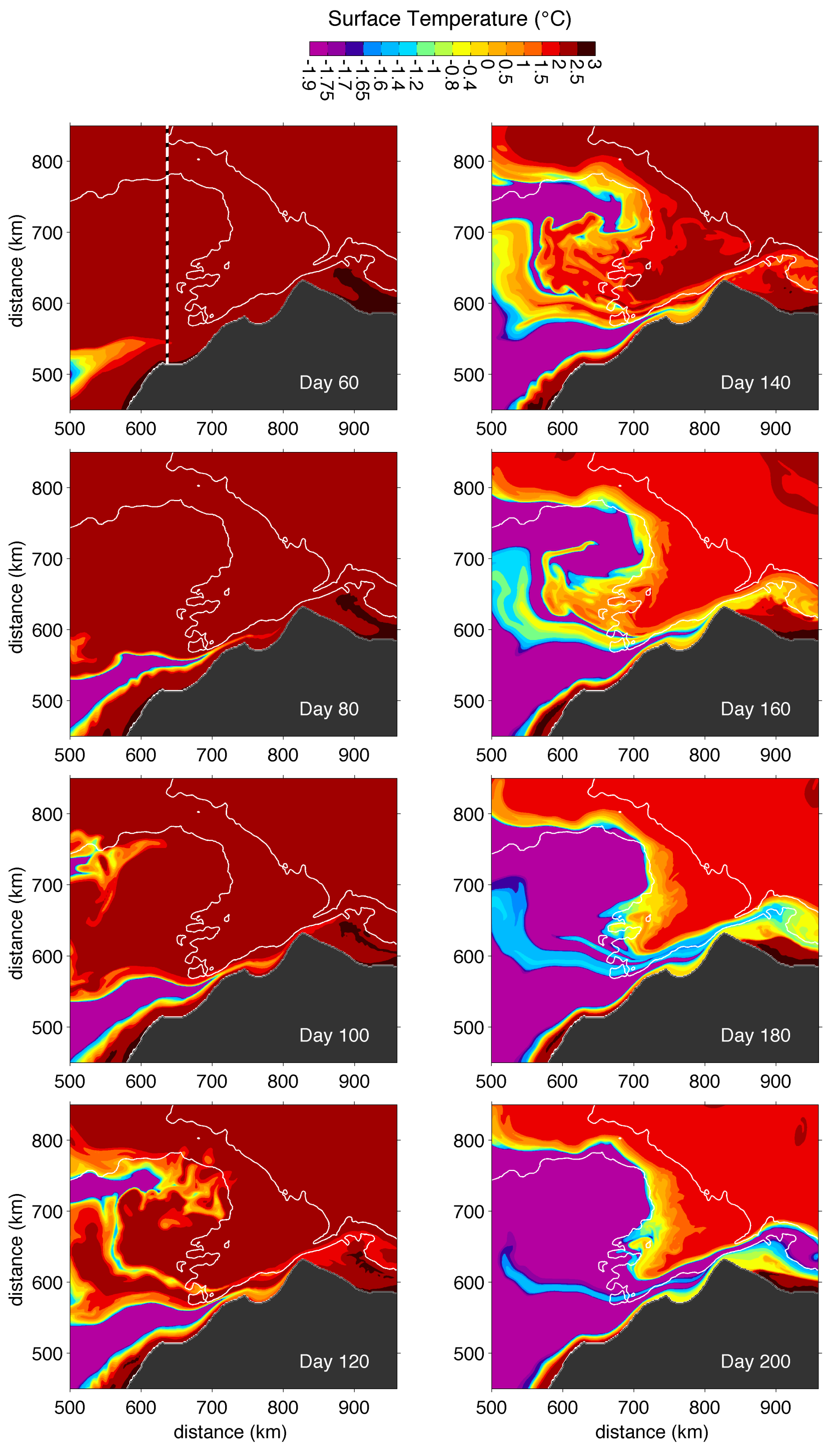

Figure 10: Surface temperature (color, °C) at specified model days in the vicinity of Barrow Canyon for the winter water simulation. The 50 and 200-m isobaths are plotted in white. The vertical line in the upper left panel indicates the location of transport estimates given in text.

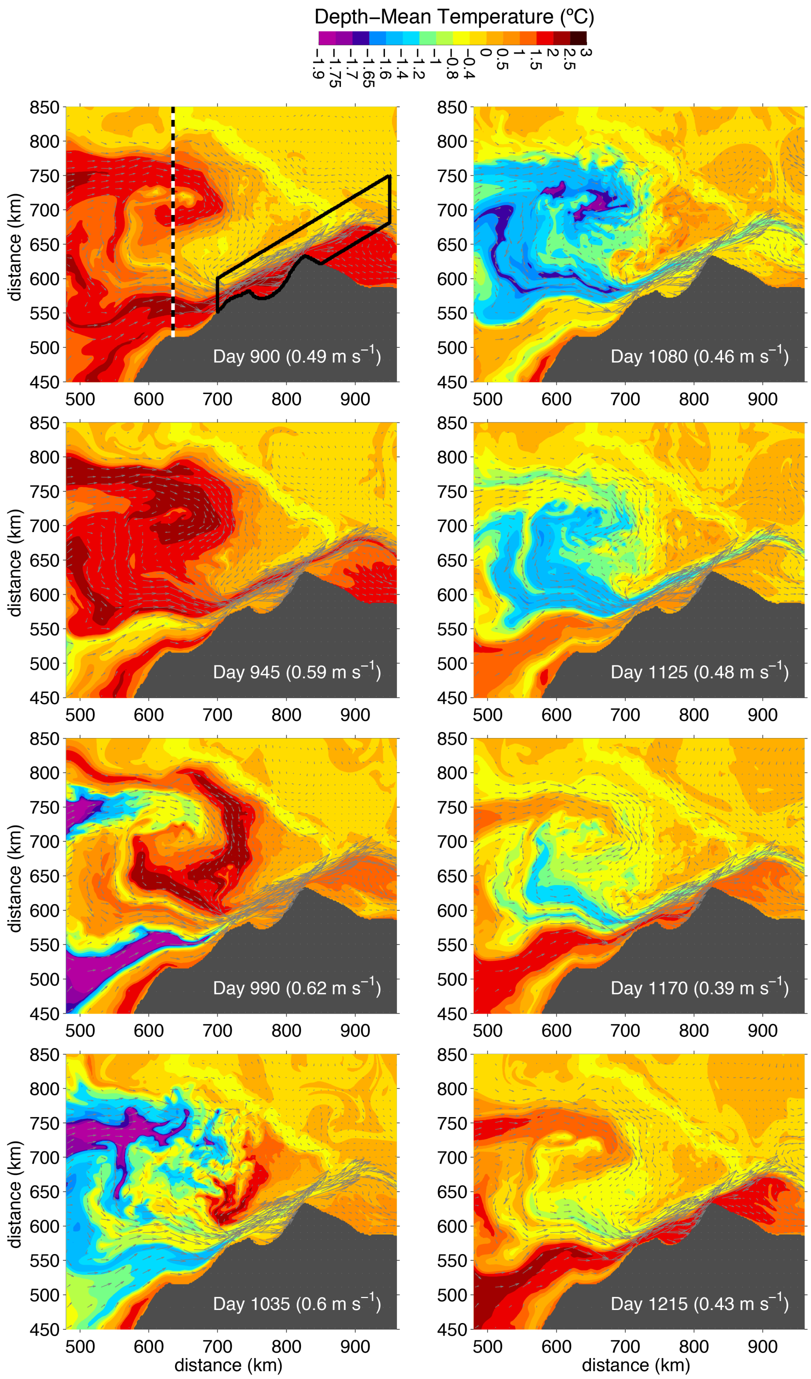

Figure 11: Depth-mean temperature (color, °C) in the vicinity of Barrow Canyon during the third year of the seasonal cycle simulation. The vectors denote the depth-mean velocity with maximum speeds indicated in the lower right corner. The upper left panel shows the transect line (dashed black-white vertical line) used to partition transports along the various pathways given in the text. The region outlined in black indicates the averaging are used in Fig. 13.

5. Comparison to the Idealized Model

The MIT general circulation model (MITgcm; Marshall et al., 1997) was used to formulate a regional oceanic model of the Chukchi Sea with realistic bathymetry (International Bathymetric Chart of the Arctic Ocean 3.0, Jakobsson et al., 2012). The horizontal resolution varied from 1-3 km, with the highest resolution centered in Barrow Canyon (Fig. 8). A 2-m vertical resolution was used within the upper 125 m of the water column; deeper than this, the resolution varied smoothly to a maximum cell size of 50 m at the model bottom depth of 525 m. The model employed a grid-dependent horizontal viscosity; typical values were around 10 m^2s^{-1}. The horizontal diffusivity was set to zero. A Mellor-Yamada (Mellor and Yamada, 1982) vertical mixing scheme was used with a background viscosity/diffusivity of 10^{-5} m^2s^{-1}. The model was initialized from rest with a horizontally uniform temperature and salinity profile created from a combination of historical CTD data for water on the shelf and ice-tethered profiler data for deeper water (Toole et al., 2011).

The eastern and western model boundaries are closed. The model was forced with a prescribed flow at the southern (Bering Strait) and northern boundaries. At both open boundaries the model temperature, salinity, and velocity are restored to prescribed values over 15 grid cells using a time constant that varied linearly from 10 days (innermost grid cell) to 1 day (outer grid cell) over the restoring region. At the northern boundary the temperature and salinity were restored to the initial conditions, and the northward velocity was set to a weak depth-uniform outflow that balanced the inflow at Bering Strait. The model is primarily forced through the southern boundary. Two simulations are considered here. The first, referred to as the winter water run, uses constant forcing at the Bering Strait defined by a uniform northward velocity of 0.2 m s^{-1} importing water near the freezing point at a salinity of 32.5. (Simulations with smaller and larger transports were also carried out, the effect of which was to lengthen/shorten the time required for the transport of winter water through the Chukchi Sea.) The winter water simulation was run for 540 days. The second simulation considers a seasonal cycle in velocity, temperature, and salinity (Fig. 8a and b) according to Woodgate et al. (2005). (We assume no spatial variation across Bering Strait.)

The climatological seasonal simulation is started in October to match the initial salinity and temperature profiles throughout the domain and was run for a total of 1260 days. Model days 15, 375, 735, and 1095, therefore, correspond to mid-October each simulation year (Fig. 8a and b).

Both simulations are formulated to consider questions related to the timing of transport pathways across the Chukchi shelf in the absence of external forcing, i.e., neglecting winds, tides, and surface heat/salt fluxes. As such, the seasonality in the model will differ from that in the observations. Importantly, however, the advective component of the model seasonal cycle driven by the Bering Strait inflow is unambiguous within the present model configuration. This allows us to robustly diagnose the travel times along the various pathways. Despite its simplifications, the model captures essential aspects of the observations in the vicinity of Barrow Canyon. In particular, the simulated current transitions from a primarily barotropic flow near the head of the canyon to a baroclinic flow with a subsurface maximum near the mouth of the canyon, as is the case for the observations (Fig. 9). In the model, this transition occurs as the dense winter water sinks to its level of neutral density as it travels down canyon. In other words, the density range encompassing the winter water mode (potential density around 26.5 kg m^{-3}) resides at an average depth of roughly 100 m in the open Beaufort Sea. The winter water simulation is also consistent with our assumption that the observed transects $BC_1(a)$, BC_2, and BC_3 are quasi-synoptic, given the similarity between the observed and modeled currents and temperature. We now use the winter water simulation to identify pathways of topographically steered flow in the vicinity of Barrow Canyon. We then consider the timing and co-existence of different water masses in Barrow Canyon using the seasonal simulation.

5.1. Transport Pathways in the Vicinity of Barrow Canyon

The winter water simulation (Fig. 10) highlights the multiple transport pathways dictated by the topography in the Chukchi Sea: a rapid route along the Alaskan coast, a slower route that circulates around the northern side of Hanna Shoal, and a third branch that diverts eastward around the southern side of Hanna Shoal. These different pathways are readily seen in the evolution of sea surface temperature (Fig. 10). The coastal branch and the clockwise circulation around the north side of Hanna Shoal have been recognized previously in models (e.g., Winsor and Chapman, 2004; Spall, 2007) and observations (Weingartner et al., 2013). Only recently has a pathway of WW around the southern side of Hanna Shoal been revealed by late-spring/early-summer shipboard measurements (Pickart et al., 2016; Pacini et al., this issue). Our model confirms such a cyclonic circulation south of the shoal (Fig. 10).

Consistent with the model of Winsor and Chapman (2004), the transit time along the coastal pathway is roughly 6 months. The WW in the central shelf pathway that is diverted south of Hanna Shoal reaches Barrow Canyon several months later, and roughly a month after this the WW in the northernmost route arrives in the canyon. Although these exact arrival times depend on the strength of the forced flow through Bering Strait, the arrival sequence is insensitive to the magnitude of the inflow (i.e., the coastal pathway is the fastest and the northern route around Hanna Shoal is the slowest.)

The eastward transport across a north-south line extending from the Alaskan coast over the top of Hanna Shoal upstream of the mouth of Barrow Canyon (x = 635 km, see the first panel of Fig. 10), indicates that the northern route around Hanna Shoal transports slightly less than half of the water (40%) that eventually drains into Barrow Canyon, with the southern two branches carrying the remaining 60%. Of this remainder, the majority of the water ($\sim$75%) is transported along the coastal pathway. While the total transport is sensitive to inflow conditions at Bering Strait, the relative ratio is consistent for the uniform winter water simulations. For a constant inflow of 0.20 m s^{-1}, the total eastward transports are 0.6 Sv for the combined coastal and southern Hanna Shoal routes and 0.4 Sv for the northern Hanna Shoal pathway. Based on data from an early-summer shipboard survey of the northeast Chukchi Sea, Pickart et al. (2016) deduced $\sim$0.8 Sv for the combined coastal and southern Hanna Shoal branches, and $\sim$0.2 Sv for the northern pathway.

5.2. Advective Seasonality of Water Masses within Barrow Canyon

The seasonal simulation allows for interpretation of the advective contribution to the seasonal cycle in the vicinity of Barrow Canyon in the absence of surface forcing (Fig. 11).

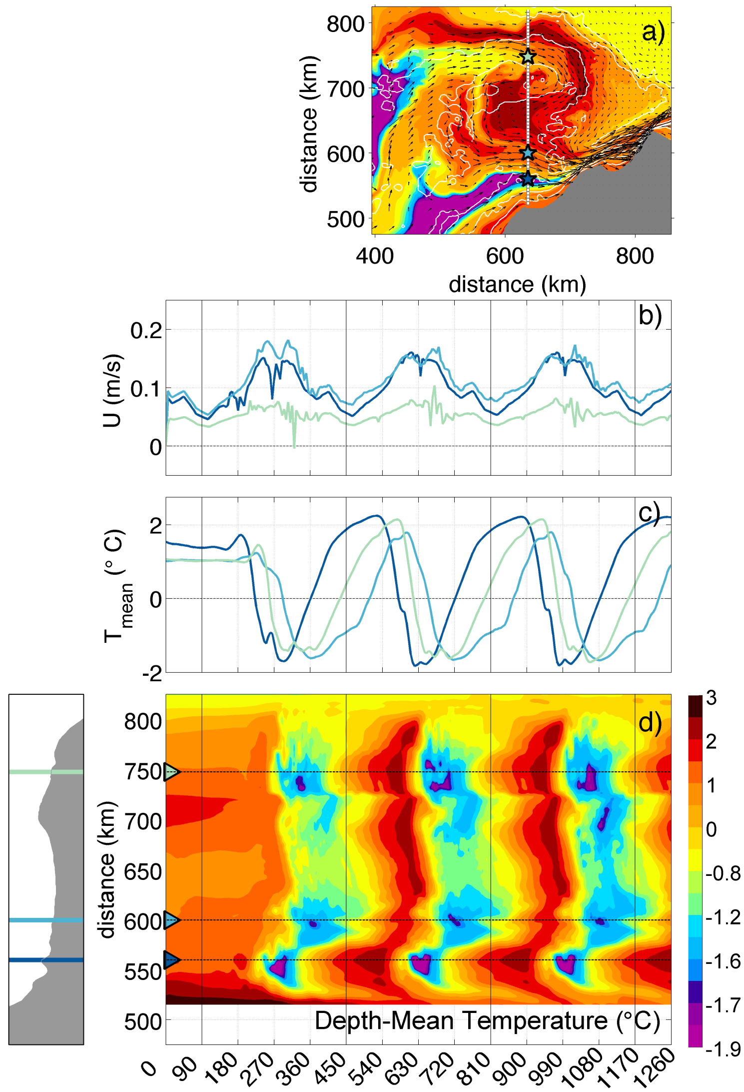

Figure 12: a) Overhead map showing the depth mean temperature (color, °C) in mid-June (model day 615). b) Time series of depth-mean eastward velocity and c) temperature at a sequence of locations progressing offshore of Alaska along a north-south transect upstream of Barrow Canyon and crossing over Hanna Shoal (x = 635 km, white dashed line in panel a). The time series locations are indicated by stars on the overhead map and horizontal lines on the bathymetric section (lower left); these locations were selected within the coastal pathway (dark blue), the southern Hanna Shoal pathway (cyan), and the northern Hanna Shoal pathway (light green). d) Depth-mean temperature (color, °C) as a function of time and transect distance. Vertical lines in b-d reference the start of model years (i.e., January 1).

The yearly progression of water mass arrival at a particular location is repeated in each model year with only slight variability in timing (order one week). Notably, the same characteristic pathways along the Alaskan coast and around the two sides of Hanna Shoal are delineated by arrival of both winter water (e.g., day 1035 in Fig. 11) and summer water (e.g. day 1215 in Fig. 11).

The advective time scales for the various pathways can be estimated by the time lag between the temperature at Bering Strait and the temperature downstream at specific locations in the Chukchi Sea. We consider three locations along the meridional line at x=635 km corresponding to the three pathways discussed above (Fig. 12a). The temperature along the northern Hanna Shoal pathway, the southern Hanna Shoal pathway, and the coastal pathway lags the forcing at Bering Strait by 200, 240, 150 days, respectively (Fig. 12c and d). The water carried along the northern Hanna Shoal route requires an additional $\sim$month to circulate clockwise around the eastern side of the shoal. From here, the northern branch must still retroflect and turn back to the east before reaching Barrow Canyon. Thus, the overall transit time through the Chukchi Sea when there is no heat exchange at the air-sea-ice interface leads to a seasonal cycle that is $\gtrsim$ 6 months out of phase with Bering Strait. In contrast to temperature (i.e., water type), the volume transports along each of the three pathways are roughly in phase with one another and vary directly with the seasonal forcing at Bering Strait (Fig. 12b). The transport adjusts nearly instantaneously across the shelf via barotropic wave propagation. (The correlations and lags mentioned above are all significant with $R \geq 0.75$.)

The time lag between the multiple pathways results in summer and winter waters regularly co-existing in the vicinity of Barrow Canyon; in fact, this is the case over the majority of the year in the model (Figs. 11 and 12). For example, as the coastal pathway transitions to summer water in the canyon, relatively cool waters are located mid-shelf (Fig. 11 day 1080). This is consistent with the observations of Pickart et al. (2016) who observed summer water in Barrow Canyon at the same time that winter water was rounding both sides of Hanna Shoal.

Although the lack of surface forcing limits realism of the overall model seasonal cycle, the simulation does indicate that winter water first arrives in the canyon via the coastal pathway, followed some time later by a second occurrence via the interior pathways. The modeled transition is demonstrated by a succession of snapshots from the simulation showing the PWW front progressing down the canyon due to the later arriving PWW from the Hanna Shoal pathways (Fig. 13). Such a rapid transition between water types draining through Barrow Canyon also offers an explanation of the abrupt change from RWW to PWW in the boundary current observations presented here (Fig. 7). Thus, we can state with confidence that the alongstream warming of the winter water observed in our shipboard survey is primarily advective in nature and not the result of mixing as the current progresses into the Beaufort Sea. The sequence of advective arrivals of varying water masses is also in line with the measurements of Weingartner et al. (2017) and Pickart et al. (this issue), as well as Weingartner et al. (2005) who argued for summertime arrival of winter water based on bottom temperature-salinity records in Barrow Canyon. Interestingly, the Weingartner et al. (2005) time series collected during the mid-1990s are suggestive of similar timing to the observations presented here, as the moored records show a pulse of PWW in late July/early August after warming earlier in the summer.

As dense winter water transits through the canyon it sinks along neutral density surfaces (Fig. 13), and the modeled current transitions from a barotropic to baroclinic structure. The simulated winter water then ventilates the upper halocline in the Beaufort where density surfaces near 26.5 kg m^{-3} are found near 100 m depth along the slope. Since the model is initialized based on the observations, it is perhaps not surprising that the observed down-canyon density field is similar to the modeled. However, it is notable that the simulated current reproduces the current structure even in the absence of wind forcing (Fig. 9). The similarity between the modeled and observed structure is again suggestive of the very important role for advection in this system— this very simple model that was tuned to examine advective influences is able to reproduce the evolution structure of the observed currents in Barrow Canyon.

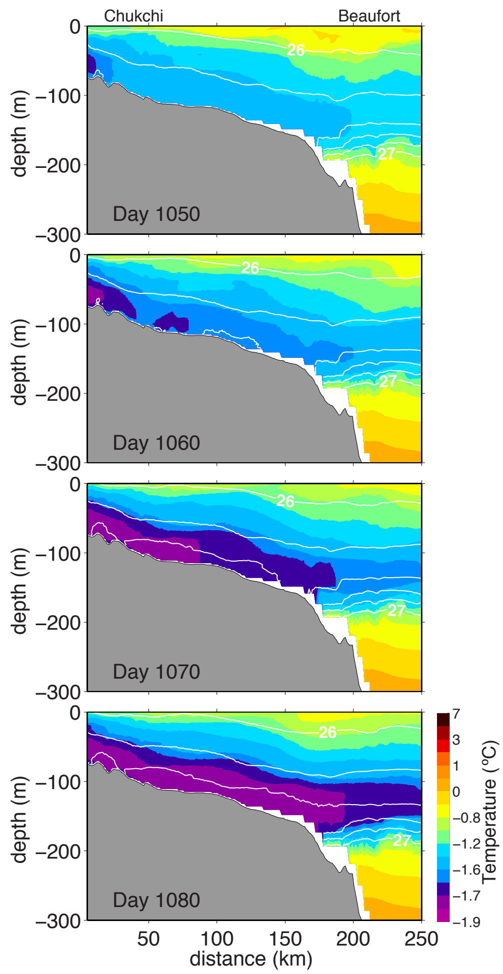

Figure 13: Along-canyon progression of the across-canyon minimum temperature, showing the transition from RWW advected by the coastal pathway (top) to PWW carried along interior pathways (bottom). White contours show potential density at 0.2 kg m^{-3} spanning the range 26-27 kg m^{-3}. An overhead view of the cross-sectional area is shown in the upper-left panel of Fig. 11 (black polygon).

6. Conclusions

Observations, supported with output from an idealized model of the Chukchi Sea, highlight the dependence of hydrographic conditions within and downstream of Barrow Canyon on the advective pathways across the Chukchi shelf. Specifically, the analyses presented here suggest that the seasonality of water masses within Barrow Canyon is closely tied to the seasonality of the Bering Strait inflow lagged by the relative transit times along three primary pathways that feed the canyon: a coastal pathway, a southern Hanna Shoal pathway, and a northern Hanna Shoal pathway. Due to the variable transit times, summer and winter water masses regularly occupy Barrow Canyon at the same time. The re-occupation of the upstream canyon transect (BC_1(b)) is especially illustrative of how different pathways advecting different water types converge within the canyon. In this case, warm Alaskan Coastal Water occupied the coastal pathway, while cold newly ventilated Pacific Winter Water (PWW) occupied the offshore flank of the canyon, having emanated from one or both of the Hanna Shoal pathways.

Analyses of wind, temperature-salinity properties, and transports suggest that the sequence of shipboard transects capturing the downstream evolution of winter water within Barrow Canyon could be treated as near-synoptic. As winter water travels down canyon, the current adjusts from a nearly barotropic structure to one with pronounced baroclinicity characterized by a sub-surface maximum in velocity. The other notable change progressing downstream was in the type of winter water mode that occupied each transect; the three upstream canyon transects (BC_{1-3}) primarily consisted of PWW, whereas BC_4 at the canyon mouth contained mostly Remnant Winter Water (RWW). While one might envision that this transition could be ascribed to alongstream mixing of PWW, Thorpe scale estimates of turbulent diffusivity suggest that such a scenario is unlikely.

Instead, we argue that the abrupt transition to RWW along the Pacific water pathway relates to the timing of the transects and drainage of different water types from the multiple pathways feeding Barrow Canyon. The mouth transect (BC_4) was sampled roughly a day after BC_2, a day prior to BC_3, and several days prior to BC_1(a). Given the advective time scales through the canyon, BC_4 was effectively sampled first in a synoptic frame. An alternative interpretation, supported by the seasonal simulation, is that PWW travelling along one (or both) of the interior shelf pathways (BC_{1-3}) was trailing RWW carried along the coastal pathway (BC_4). The model suggests that such a transition occurs on the order of one week, while the observations indicate that it can happen in a matter of days.

Even though the above analyses suggest that local diapycnal mixing does not solely create the observed RWW, the Thorpe scale estimates of dissipation and diffusivity are not negligible – just insufficient to locally produce the observed volume of RWW. Mixing (both isopycnal and diapycnal) may have other important, yet more subtle, consequences. For example, given that a portion of the water emanating from Barrow Canyon moves directly into the deep Canada Basin and Beaufort Sea, local turbulent buoyancy fluxes may modify how and where the Arctic halocline is ventilated. Furthermore, since topographically steered waters have different origins as well as advective histories, dissimilar water types that co-exist in the canyon will likely be distinguished by properties other than temperature and salinity, such as carbon and nutrients. Turbulent flux divergence may therefore be an important contributor to other tracer budgets. For example, a straightforward extension is that mixing between nutrient replete and deplete waters may help sustain this biologically productive region (e.g., Grebmeier et al., 2006). The combination of advection leading to heterogenous water properties over a constrained geographic region, and local mixing acting on pronounced gradients, lead to the potential for Barrow Canyon to play a central role in regional water mass modification.

Acknowledgements

The authors thank Terry McKee for calibrating the hydrographic data and Frank Bahr for processing the shipobard ADCP data set. ES was supported as a WHOI Postdoctoral Scholar through the WHOI Ocean and Climate Change Institute and under the National Science Foundation under grant 1734777. RP was funded by the National Science Foundation under grant PLR-1303617.

References

Aagaard K, Roach AT. Arctic ocean-shelf exchange: Measurements in Barrow Canyon. J Geophys Res 1990;95:18163–75. doi:10.1029/JC095iC10p18163.

Bourke RH, Paquette RG. Atlantic Water on the Chukchi Shelf. Geophys Res Let 1976;3(10):629–32.

Brugler ET, Pickart RS, Moore GWK, Roberts S, Weingartner TJ, Statscewich H. Seasonal to interannual variability of the Pacific water boundary current in the Beaufort Sea. Progress in Oceanography 2014;127:1–20.

Coachman LK, Aagaard K, Tripp RB. Bering Strait: The regional physical oceanography. University of Washington Press, 1975.

Codispoti LA, Flagg C, Kelly V, Swift JH. Hydrographic conditions during the 2002 sbi process experiments. Deep Sea Research Part II: Topical Studies in Oceanography 2005;52(24):3199–226. URL: http://www.sciencedirect.com/science/article/pii/S0967064505002171. doi:https://doi.org/10.1016/j.dsr2.2005.10.007.

Corlett W, Pickart RS. The Chukchi Slope Current. Progress in Oceanography 2017;153:50–6.

Dillon TM. Vertical overturns: A comparison of Thorpe and Ozmidov length scales. J Geophys Res 1982;87(C12):9601–13.

Galbraith PS, Kelley DE. Identifying overturns in CTD profiles. J Atmos Ocean Technol 1996;13:688–702.

Gong D, Pickart RS. Summertime circulation in the eastern Chukchi Sea. Deep Sea Research Part II: Topical Studies in Oceanography 2015;118:18–31.

Grebmeier JM, Bluhm BA, Cooper LW, Danielson SL, Arrigo KR, Blanchard AL, Clarke JT, Day RH, Frey KE, Gradinger RR, Kedra M, Konar B, Kuletz KJ, Lee SH, Lovvorn JR, Norcross BL, Okkonen SR. Ecosystem characteristics and processes facilitating persistent macrobenthic biomass hotspots and associated benthivory in the pacific arctic. Progress in Oceanography 2015;136(Supplement C):92–114. URL: http://www.sciencedirect.com/science/article/pii/S0079661115001032. doi:https://doi.org/10.1016/j.pocean.2015.05.006.

Grebmeier JM, Cooper LW, Feder HM, Sirenko BI. Ecosystem dynamics of the Pacific-influenced Northern Bering and Chukchi Seas in the Amerasian Arctic. Progress in Oceanography 2006;71:331–61. doi:10.1016/j.pocean.2006.10.001.

Hill V, Cota G. Spatial patterns of primary production on the shelf, slope and basin of the western arctic in 2002. Deep Sea Research Part II: Topical Studies in Oceanography 2005;52(24):3344–54. URL: http://www.sciencedirect.com/science/article/pii/S0967064505002249. doi:https://doi.org/10.1016/j.dsr2.2005.10.001.

Itoh, M. and Shimada, K. and Kamoshida, T. and McLaughlin, F. and Carmack, E. and Nishino, S. . Interannual variability of Pacific Winter Water inflow through Barrow Canyon from 2000 to 2006. J Oceanogr 2012;68:575–92. doi:10.1007/s10872-012-0120-1.

Jakobsson M, Mayer L, Coakley B, Dowdeswell JA, Forbes S, Fridman B, Hodnesdal H, Noormets R, Pedersen R, Rebesco M, Schenke HW, Zarayskaya Y, Accettella D, Armstrong A, Anderson RM, Bienhoff P, Camerlenghi A, Church I, Edwards M, Gardner JV, Hall JK, Hell B, Hestvik O, Kristoffersen Y, Marcussen C, Mohammad R, Mosher D, Nghiem SV, Pedrosa MT, Travaglini PG, Weatherall P. The International Bathymetric Chart of the Arctic Ocean (IBCAO) Version 3.0. Geophysical Research Letters 2012;39(12). URL: http://dx.doi.org/10.1029/2012GL052219. doi:10.1029/2012GL052219.

Ladd C, Mordy CW, Salo SA, Stabeno PJ. Winter water properties and the Chukchi polynya. J Geophys Res 2016;121:5516–34.

Li M, Pickart RS. Circulation of the chukchi sea shelfbreak and slope from moored timeseries. Arctic Marine Science Symposium 2017;Abstract, pg 85, http://www.nprb.org/assets/amss/images/uploads/files/AMSS2017_BookofAbstracts.pdf.

Lin P, Pickart R, Moore G, Spall M, Hu J. Characteristics and dynamics of wind-driven upwelling in the Alaskan Beaufort Sea based on six years of mooring data. Deep Sea Res II this issue;.

Lowry KE, Pickart RS, Mills MM, Brown ZW, van Dijken GL, Bates NR, Arrigo KR. The influence of winter water on phytoplankton blooms in the chukchi sea. Deep Sea Research Part II: Topical Studies in Oceanography 2015;118(Part A):53–72. URL: http://www.sciencedirect.com/science/article/pii/S0967064515002064. doi:https://doi.org/10.1016/j.dsr2.2015.06.006.

Marshall J, Adcroft A, Hill C, Perelman L, Heisey C. A finite-volume, incompressible Navier Stokes model for studies of the ocean on parallel computers. J Geophys Res 1997;102:5753–66. doi:10.1029/96JC02775.

Mellor GL, Yamada T. Developement of a turbulence closure model for geophysical fluid problems. Rev Geophys Space Phys 1982;20:851–75.

Moore S, Grebmeier J. The distributed biological observatory: Linking physics to biology in the pacific arctic region. Arctic 2017;.

Mountain DG, Coachman LK, Aagaard K. On the flow through Barrow Canyon. J Phys Ocean 1976;6:461–70. doi:{10.1175/1520-0485(1976)006<0461:OTFTBC>2.0.CO;2}.

Muench RD, Schumacher JD, Salo SA. Winter currents and hydrographic conditions on the northern central Bering Sea shelf. J Geophys Res 1988;93:516–26.

Münchow A, Carmack EC. Synoptic Flow and Density Observations near an Arctic Shelf Break. J Phys Ocean 1997;27:1402–19. doi:10.1175/1520-0485(1997)027<1402:SFADON>2.0.CO;2.

Nikolopoulos A, Pickart RS, Fratantoni PS, Shimada K, Torres DJ, Jones EP. The western arctic boundary current at 152 ° W: Structure, variability, and transport. Deep Sea Res II 2009;56:1164–81.

Okkonen SR, Ashjian CJ, Campbell RG, Maslowski W, Clement-Kinney JL, Potter R. Intrusion of warm Bering/Chukchi waters onto the shelf in the western Beaufort Sea. J Geophys Res 2009;114(C13):0–+. doi:10.1029/2008JC004870.

Pacini A, Pickart R, Moore G, Nobre C, Bahr F, Vage K, Arrigo K. Characteristics and transformation of pacific winter water on the Chukchi Sea shelf in late-spring. Deep Sea Res II this issue;.

Padman L, Erofeeva S. A barotropic inverse tidal model for the Arctic Ocean. Geophys Res Let 2004;31:2303. doi:10.1029/2003GL019003.

Pickart R, Moore G, Mao C, Bahr F, Nobre C, Weingartner T. Circulation of winter water on the Chukchi shelf in early summer. Deep Sea Res II 2016;130:56–75.

Pickart R, Nobre C, Lin P, Arrigo K, Ashjian C, Berchok C, Cooper L, Grebmeier J, Hartwell I, He J, Itoh M, Kikuchi T, Nishino S, Vagle S. Seasonal to mesoscale variability of water masses and atmospheric conditions in Barrow Canyon, Chukchi Sea. Deep Sea Res II this issue;.

Pickart RS, Stossmeister G. Outflow of Pacific water from the Chukchi sea to the Arctic Ocean. J Phys Ocean 2008;10:135–48.

Pickart RS, Weingartner TJ, Pratt LJ, Zimmermann S, Torres DJ. Flow of winter-transformed Pacific water into the Western Arctic. Deep Sea Res 2005a;52:3175–98.

Pickart RS, Weingartner TJ, Pratt LJ, Zimmermann S, Torres DJ. Flow of winter-transformed Pacific water into the Western Arctic. Deep Sea Res 2005b;52:3175–98. doi:10.1016/j.dsr2.2005.10.009.

Pisareva M, Pickart R, Fratantoni P, Weingartner T. On the nature of wind-forced upwelling in Barrow Canyon. Deep Sea Res II this issue;.

Pisareva M, Pickart R, Spall M, Nobre C, Torres D, Moore G. Flow of pacific water in the western Chukchi Sea: Results from the 2009 RUSALCA expedition. Deep Sea Res 2015;105:53–73.

Schulze LM, Pickart RS. Seasonal variation of upwelling in the Alaskan Beaufort Sea: Impact of sea ice cover. J Geophys Res (Oceans) 2012;117(C16):C06022. doi:10.1029/2012JC007985.

Shroyer EL. Turbulent kinetic energy dissipation in barrow canyon. J Phys Oceanogr 2012;42:1012–21. doi:10.1175/JPO-D-11-0184.1.

Shroyer EL, Plueddemann AJ. Wind-driven modification of the alaskan coastal current. J Geophys Res 2012;117(C03031). doi:10.1029/2011JC007650.

Spall MA. Circulation and water mass transformation in a model of the Chukchi Sea. J Geophys Res 2007;112(C11):5025–+. doi:10.1029/2005JC003364.

Steele M, Morison J, Ermold W, Rigor I, Ortmeyer M, Shimada K. Circulation of summer Pacific halocline water in the Arctic Ocean. J Geophys Res 2004;109(C02027). doi:10.1029/2003JC002009.

Thorpe SA. Turbulence and mixing in a Scottish Loch. Philos Trans Roy Soc London 1977;286(1334):125–81.

Toole J, Krishfield R, Timmermans ML, Proshutinsky A. The Ice-Tethered Profiler: Argo of the Arctic. Oceanography 2011;24(3):126–35.

Weingartner T. J. ea. Hydrographic variability over the northeastern chukchi sea shelf in summer-fall 2008-2012. Continental Shelf Research 2012;67:5–22.

Weingartner T, Aagaard K, Woodgate R, Danielson S, Sasakic Y, Cavalieri D. Circulation on the north central Chukchi Sea shelf. Deep Sea Res 2005;52:3150–74.

Weingartner T, Dobbins E, Danielson S, Winsor P, Potter R, Statscewich H. Hydrographic variability over the northeastern Chukchi Sea shelf in summer-fall 2008–2010. Cont Shelf Res 2013;67:5–22.

Weingartner TJ, Cavalieri DJ, Aagaard K, Sasaki Y. Circulation, dense water formation, and outflow on the northeast Chukchi shelf. J Geophys Res 1998;103:7647–62. doi:10.1029/98JC00374.

Weingartner TJ, Potter RA, Stoudt CA, Dobbins EL, Statscewich H, Winsor PR, Mudge TD, Borg K. Transport and thermohaline variability in barrow canyon on the northeastern chukchi sea shelf. Journal of Geophysical Research: Oceans 2017;122(5):3565–85. URL: http://dx.doi.org/10.1002/2016JC012636. doi:10.1002/2016JC012636.

Winsor P, Chapman DC. Pathways of Pacific water across the Chukchi Sea: A numerical model study. J Geophys Res 2004;109(C18):3002–+. doi:10.1029/2003JC001962.

Woodgate RA, Aagaard K. Revising the Bering Strait freshwater flux into the Arctic Ocean. Geophys Res Let 2005;32:2602–+. doi:10.1029/2004GL021747.

Woodgate RA, Aagaard K, Weingartner TJ. A year in the physical oceanography of the Chukchi Sea: Moored measurements from autumn 1990 1991. Deep Sea Research Part II: Topical Studies in Oceanography 2005;52:3116–49. doi:10.1016/j.dsr2.2005.10.016.